LETTER

doi:10.1038/nature11215

Structured spheres generated by an in-fibre fluid instability

Joshua J. Kaufman[1], Guangming Tao[1], Soroush Shabahang[1], Esmaeil-Hooman Banaei[1,2], Daosheng S. Deng[3], Xiangdong Liang[4], Steven G. Johnson[4], Yoel Fink[5] & Ayman F. Abouraddy[1]

From drug delivery[1,2] to chemical and biological catalysis[3] and cosmetics[4], the need for efficient fabrication pathways for particles over a wide range of sizes, from a variety of materials, and in many different structures has been well established[5]. Here we harness the inherent scalability of fibre production[6] and an in-fibre Plateau–Rayleigh capillary instability[7] for the fabrication of uniformly sized, structured spherical particles spanning an exceptionally wide range of sizes: from 2 mm down to 20 nm. Thermal processing of a multimaterial fibre[8] controllably induces the instability[9], resulting in a well-ordered, oriented emulsion[10] in three dimensions. The fibre core and cladding correspond to the dispersed and continuous phases, respectively, and are both frozen *in situ* on cooling, after which the particles are released when needed. By arranging a variety of structures and materials in a macroscopic scaled-up model of the fibre, we produce composite, structured, spherical particles, such as core–shell particles, two-compartment 'Janus' particles[11], and multi-sectioned 'beach ball' particles. Moreover, producing fibres with a high density of cores allows for an unprecedented level of parallelization. In principle, 10^8 50-nm cores may be embedded in metres-long, 1-mm-diameter fibre, which can be induced to break up simultaneously throughout its length, into uniformly sized, structured spheres.

Bottom-up approaches to particle synthesis—through nucleation, chemical reactions or self-assembly[12,13]—yield nanometre-scale particles from a variety of materials. The particles produced using such approaches are typically characterized by a large dispersion in the size distribution, and are hampered by coalescence and agglomeration during particle growth. Producing complex multimaterial structures or mono-disperse micro-sized particles is technologically challenging in bottom-up synthesis approaches. On the other hand, top-down approaches[14]—such as microfluidics[15,16], lithography[17,18] and imprint lithography[19]—typically yield larger, mono-disperse particles, but are each suited to a specific material and size range determined by the underlying kinetics of the process. Lithography and imprint lithography produce nanoparticles at low rates, because the produced volume scales with particle size in two-dimensional processes. Furthermore, fabricating structured spherical particles requires non-trivial modifications to these approaches, which ultimately impose constraints on the number of geometric features and types of material combined in a particle. Our new, scalable process exploits a fluid instability occurring within a multimaterial fibre to produce a necklace of spherical particles inside the fibre, with complex geometries combining multiple materials, made with the same ease as producing single-material particles.

Figure 1 outlines our approach to particle generation. The procedure starts with the preparation of a macroscopic scale model, called a 'preform', whose core is assembled from the intended particle constituent materials encased in a supporting cladding. The preform is then thermally drawn into an extended fibre[6,8], until the core diameter approaches the required particle size (Fig. 1a). Figure 1b shows an example of a fibre cross-section, comprising an amorphous, semiconducting chalcogenide glass core (As_2Se_3) encased in a polymer cladding (polyethersulphone, PES); see Supplementary Information section 1 for details. To ensure the integrity of the core, the preform is thermally drawn in a high-viscosity regime ($>10^6$ Pa s), and the fibre emerging from the heating zone is cooled quickly to arrest the development of any axial instability. This drawing process produces axially stable cores[20] with diameters from >1 mm to <3 nm, which sets the upper and lower limits on the potential particle sizes.

Thermal treatment of this fibre induces the Plateau–Rayleigh instability (PRI)[7,9], resulting in the breakup of the continuous core into an orderly arrangement of spherical particles held immobile in the cladding. We capture the full dynamics of the breakup process by applying a temperature gradient along the axis of a fibre section (Fig. 1c). At the low-temperature end (left-hand side), the highly viscous core remains intact. As temperature increases (and viscosity decreases; right-hand side), surface tension dominates and a sinusoidal modulation develops at the core–cladding interface, leading ultimately to the breakup of the core into a string of spherical particles. When we heat the fibre uniformly for sufficient time, the PRI develops globally along its whole length (Supplementary Fig. 1). In contrast to the rapid cooling after fibre drawing, the stationary fibre is maintained at elevated temperature for an extended period of time, allowing the core to break up into uniformly sized droplets which are frozen *in situ* on cooling. The particles may be subsequently released when needed by dissolving the cladding. Our approach is a thermally driven emulsification of dispersed-phase particles (derived from the core) suspended in an immiscible continuous-phase fluid (the cladding)[21]. The core may be considered a pre-filled fluidic channel[15], filled during the construction of the centimetre-scale preform in the solid state, which is reduced to a high-viscosity fluid during the fibre draw and subsequent thermal processing.

This approach to particle fabrication by multimaterial in-fibre emulsification has several important features. First, it can produce uniformly sized spherical particles over an extremely wide range of diameters. This may be appreciated by modelling the fibre core at elevated temperature as a viscous fluid thread surrounded by an infinitely extended viscous immiscible fluid, and making use of the classical Tomotika linear stability theory[22] to calculate the instability growth time τ for potential instability wavelengths λ (see Supplementary Information section 5). We obtain the fastest-growing λ (corresponding to the smallest τ) at which the breakup is favoured to occur for different values of temperature T and core diameter D (Fig. 1d). In general, τ is linearly proportional to D and inversely dependent on T. In this model, a core will break up, at any fixed T, after heating for a sufficiently long time. We have drawn fibres with core diameters ranging from $\sim$2 mm down to 20 nm (Supplementary Information section 1) and used them to produce particles with perfectly spherical and exquisitely smooth-surfaced

[1]CREOL, The College of Optics & Photonics, University of Central Florida, Orlando, Florida 32816, USA. [2]Department of Electrical Engineering & Computer Science, University of Central Florida, Orlando, Florida 32816, USA. [3]Department of Chemical Engineering, Massachusetts Institute of Technology, Cambridge, Massachusetts 02139, USA. [4]Department of Mathematics, Massachusetts Institute of Technology, Cambridge, Massachusetts 02139, USA. [5]Department of Materials Science and Engineering, Massachusetts Institute of Technology, Cambridge, Massachusetts 02139, USA.

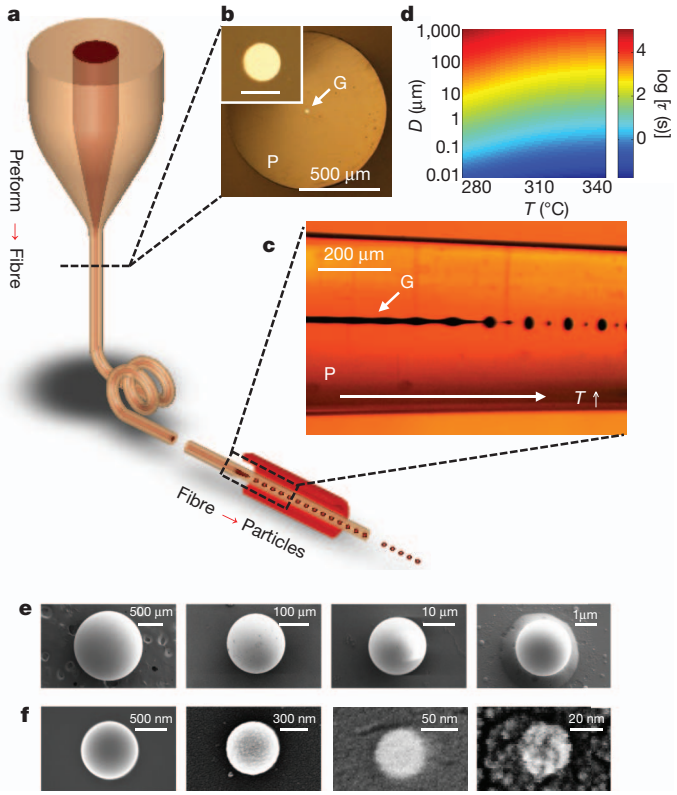

Figure 1 | Fluid capillary instabilities in multimaterial fibres as a route to size-tunable particle fabrication. **a**, A macroscopic preform is thermally drawn into a fibre. Subsequent thermal processing of the fibre induces the PRI, which results in the breakup of the intact core into spherical droplets that are frozen *in situ* on cooling. **b**, Reflection optical micrograph of a fibre cross-section with 20-μm-diameter core; inset shows the core (scale bar, 20 μm). The fibre consists of an As_2Se_3 glass core (G), encased in a PES polymer cladding (P). **c**, Transmission optical micrograph of the fibre side-view in **b** after a temperature (T) gradient is applied along the axis to induce the PRI at the core–cladding interface. **d**, Calculated instability time, τ, for various temperatures T and core diameters D (see Supplementary Information). **e**, SEM images of microparticles with diameters of ~1.4 mm, 200 μm, 18 μm and 2.7 μm. **f**, SEM images of nanoparticles with diameters of ~920, 560, 62 and 20 nm.

external morphology over the entire range of diameters (Fig. 1e, f), confirmed by scanning electron microscope (SEM) imaging after dissolving the polymer cladding using dimethylacetamide[23]. This range corresponds to five orders of magnitude in linear dimension—fifteen in volume, from ~8 mm^3 to ~8,000 nm^3. The polydispersity of the particle distribution for targeted micro- and nanoparticle sizes was determined using dynamic light scattering, and the standard deviation normalized with respect to the mean of the size distribution was found to be ~10% (see Supplementary Fig. 2 for details).

The second key aspect of the in-fibre process is its scalability—that is, the ability to produce large numbers of particles by parallelizing the simultaneous breakup of a high density of cores occupying the same long fibre. Starting from a macroscopic rod, one may in principle convert its entirety into particles of prescribed size. Using a stack-and-draw approach, we have produced fibres of 1 mm outer diameter, containing 12 20-μm cores (Fig. 2a and Supplementary Fig. 3), 4,000 500-nm cores, or 27,000 200-nm cores (Fig. 2d, Supplementary Figs 4, 5; Supplementary Table 1). In principle, one may combine 10^8 50-nm cores in such a fibre with 25% fill factor. This far exceeds the current parallelization capabilities of microfluidics-based approaches[24]. Furthermore, the resulting spatial distribution of particles held immobilized in the scaffold is well-ordered in three dimensions (Fig. 2b, Supplementary Fig. 6). In the axial direction the particles are ordered because the instability growth is dominated by a single wavelength. In the transverse dimensions, order is imposed on the cores during the stacking process (Supplementary Figs 3–6).

The third characteristic is the ease by which this top-down process may be configured to produce structured particles. Because the preform is constructed at the centimetre scale, complex preform geometries may be readily designed and realized, so that the PRI-driven breakup in the drawn fibre produces a desired particle structure. We demonstrate here the size-controllable fabrication of spherical core–shell particles (Fig. 3) and 'Janus' particles (Fig. 4). The preform used to produce the core–shell particles (corresponding to a double emulsion[15]) consists of a polymer core (diameter D_1) and glass cladding (diameter $D_2 \approx 2.5 \times D_1$), surrounded by a polymer matrix (Fig. 3a; cross-sections shown in Fig. 3b, c). The polymer core and glass shell undergo a correlated PRI-driven breakup that results in core–shell particles, observed experimentally (Fig. 3d, e) and confirmed through simulations (Fig. 3f). To confirm that the PRI-driven breakup produces the

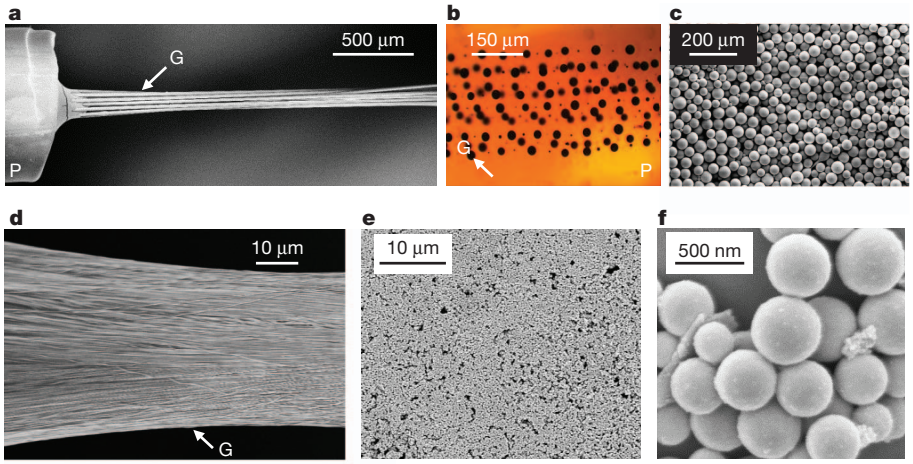

Figure 2 | Scalable fabrication of micro- and nano-scale spherical particles. **a**, SEM micrograph of 12 20-μm intact glass cores (G, As_2Se_3), exposed from a 1-mm-diameter fibre after dissolving the polymer cladding (P, PES). An SEM micrograph of the fibre cross-section is shown in Supplementary Fig. 3. **b**, Transmission optical micrograph of the fibre side-view, showing the cores after global heating of the fibre, which results in the simultaneous breakup of the cores into an ordered distribution of particles in three dimensions held in the polymer cladding. **c**, SEM micrograph of a large number of 40-μm (average diameter) glass particles released from the fibre in **b** by dissolving the polymer cladding. **d**, SEM micrograph of 27,000 200-nm-diameter intact glass cores exposed from a 1-mm-diameter fibre. An SEM micrograph of the fibre cross-section is shown in Supplementary Figs 4, 5. **e**, SEM micrograph of a large number of 400-nm (average diameter) glass particles. **f**, SEM micrograph of a few particles from **e**. See Supplementary Fig. 2 for the particle-size distribution.

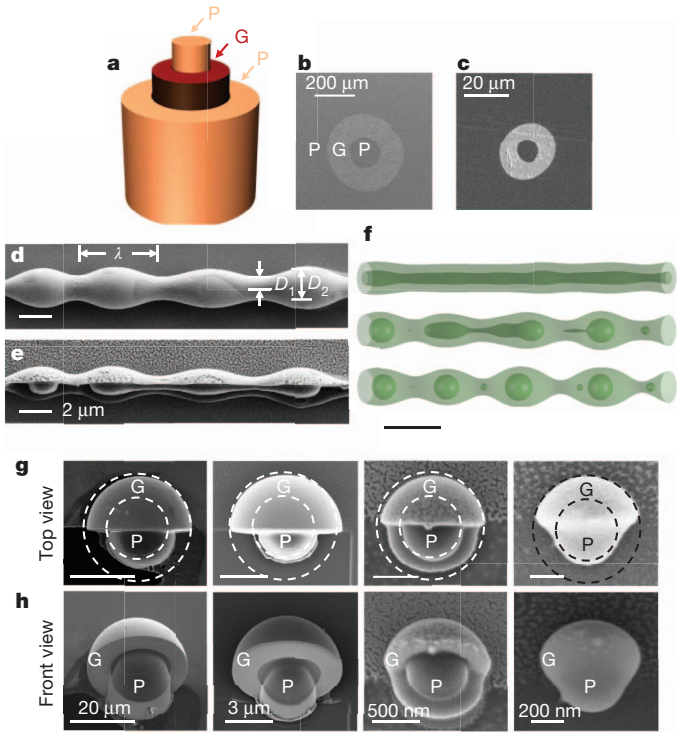

Figure 3 | Polymer-core/glass-shell spherical particle fabrication. **a**, Schematic of the fibre structure (P, G as in Figs 1, 2). **b**, **c**, SEM images of fibre cross-sections. **d**, SEM image of the glass-shell outer surface, showing the modulation characteristic of the PRI. **e**, SEM image of the structure in **d** after sectioning off half of the glass shell using a focused ion beam (FEI 200 THP; current ~10–100 pA), revealing the correlated modulations on the two interfaces (inner polymer/glass and outer glass/polymer interfaces), and resulting ultimately in two concentric spherical surfaces as shown in **g** and **h**. **f**, Three snapshots from a three-dimensional simulation of the Stokes equations using a representative fibre structure (full movie available online; see Supplementary Information), illustrating the full breakup process. Time progresses from top to bottom. Scale bar, 50 μm. Dark green, polymer core; light green, glass shell; the outer polymer scaffold cladding is made transparent for clarity. **g**, Top and **h**, front (tilted) SEM views of four differently sized core–shell particles (outer diameters 34 μm, 7 μm, 1.2 μm and 650 nm, respectively). Scale bars in the corresponding top and front views are the same length.

expected structure, we use a focused ion beam (FIB) to 'slice' the particle down the middle by raster-scanning the FIB across a box with an edge lying through the particle. The FIB etches the semiconducting glass shell, with its higher electrical conductivity, more effectively than the insulating polymer core. Figure 3g, h shows SEM images of particles with outer diameters from 35 μm to 600 nm (the FIB damages the smaller particles that we produced), showing the intact polymer core protruding from the remaining glass half-shell. Figure 3g, h confirms the smooth core/shell interface, the particles' concentric spherical surfaces, and that the expected core/shell diameter ratio is $D_1'/D_2' = (D_1/D_2)^{2/3}$, as dictated by conservation of volume (where D_1' and D_2' are the particle core and shell diameters, respectively). Since $D_1/D_2 = 0.4$ (Fig. 3b, c), we expect $D_1'/D_2' \approx 0.543$, in close agreement with the measured value of ~0.575 (Fig. 3g).

We quantitatively analyse the breakup process in this nested, cylindrical, multi-fluid structure using linear stability analysis[25] to determine the exponential growth rates of small sinusoidal perturbations. The dominant breakup wavelength is plotted as a function of the core/shell viscosity ratio in Supplementary Fig. 7. The predicted and measured breakup length scales are consistent, within the experimental uncertainties in D_1 and viscosity contrast. To study the dynamics of the full breakup process, we performed full three-dimensional simulations of the Stokes equations (valid here because the Reynolds number is low[26]), using a level-set/spectral method[25]. For illustration purposes we used equal core and shell viscosities (10^5 Pa s, corresponding to $T \approx 270\,^{\circ}$C) and an initial diameter $D_1 = 23$ μm. Three snapshots of the simulation, starting from white-noise initial perturbations, are shown in Fig. 3f (full movie available online). The inner interface breaks up first, as predicted from stability analysis and observed experimentally (Fig. 3d, e), and we also occasionally observe small 'satellite' droplets forming among the larger droplets.

The second structured particle we produce is a broken-symmetry, spherical Janus particle, comprising two hemispheres of different optical glasses (Fig. 4). The preform core is constructed of two half cylinders, each of a different semiconducting glass with distinct complex refractive index: G1 (As_2S_3) and G2 ($(As_2Se_3)_{99}Ge_1$) (Fig. 4a–c; Supplementary Information section 7). The induced breakup produces spherical Janus particles held immobilized with the same orientation in the cladding (Fig. 4d). Figure 4e shows a reflection optical micrograph of a single Janus particle removed from the cladding. We confirm the three-dimensional structure of the particle by optically imaging multiple parallel planes cutting through a particle still embedded in the polymer cladding (Fig. 4f), and correlating the optical images with energy-dispersive X-ray diffraction (EDX) spectral images of the particle cross-section (Fig. 4g) that identify arsenic and sulphur. The measurements confirm the three-dimensional, two-compartment structure of the Janus particle.

Modelling Janus-particle formation is difficult because it involves a point where three fluids meet, so that sophisticated level-set techniques are required to describe the interfaces[27]. The physics of such a contact point is not well understood[28], although it is likely to be less relevant in the Stokes regime[29,30]. Nevertheless, energy considerations yield some qualitative predictions. A large glass–glass surface tension, compared to that between glass and polymer, would make it energetically favourable for the Janus particles to pinch in the centre. On the other hand, for negligible glass–glass tension, if the glass–polymer surface tension were very different for the two glasses, energy would be lowered if one glass were to flow to envelop the other. As neither of these scenarios is observed experimentally (Fig. 4d, e), we can conclude that the observed breakup process is consistent with low glass–glass surface tension and similar glass–polymer tensions. These considerations indicate a general strategy for the construction of particles with even more complex geometry. Furthermore, to form two-component particles, the viscosities of the two materials must be matched; we identify pairs of compatible materials by looking for overlapping softening temperatures.

The two particle structures considered above, the core–shell and two-compartment Janus particles, are prototypical structures from which more complex geometries may be constructed. For example, multilayer particles may be produced using a core consisting of nested cylindrical shells of appropriate thicknesses, and additional azimuthal compartments in the particle result from a core appropriately prepared with azimuthal sections. Furthermore, these two prototypical structures may be combined in the same particle. The power of this approach is highlighted in Fig. 4h–k, which shows the fabrication of a 'beach ball' particle, consisting of six equally sized wedge-shaped sections of alternating materials (G1 and G2). The preform consists of a cylindrical core with six equally sized segments, each subtending a 60° polar angle. More complex particle structures may be produced by judiciously structuring the core.

This process uses thermally compatible material systems dominated by viscous forces and surface tension, such as glasses, polymers, metals above their melting temperature, and liquids. An example of breakup in an all-polymer fibre is shown in Supplementary Fig. 10. Moreover, drawing multimaterial fibres with crystalline semiconductor cores[31] (silicon, germanium and III–V binary compounds) and the synthesis of new materials during fibre drawing[32] indicate the possibility of extending our methodology to a wider range of materials. Finally, fibre fabrication technology produces kilometres of fibre in a few hours[6], with a total core mass of 1 kg that is potentially converted entirely into particles, with each metre of fibre containing up to

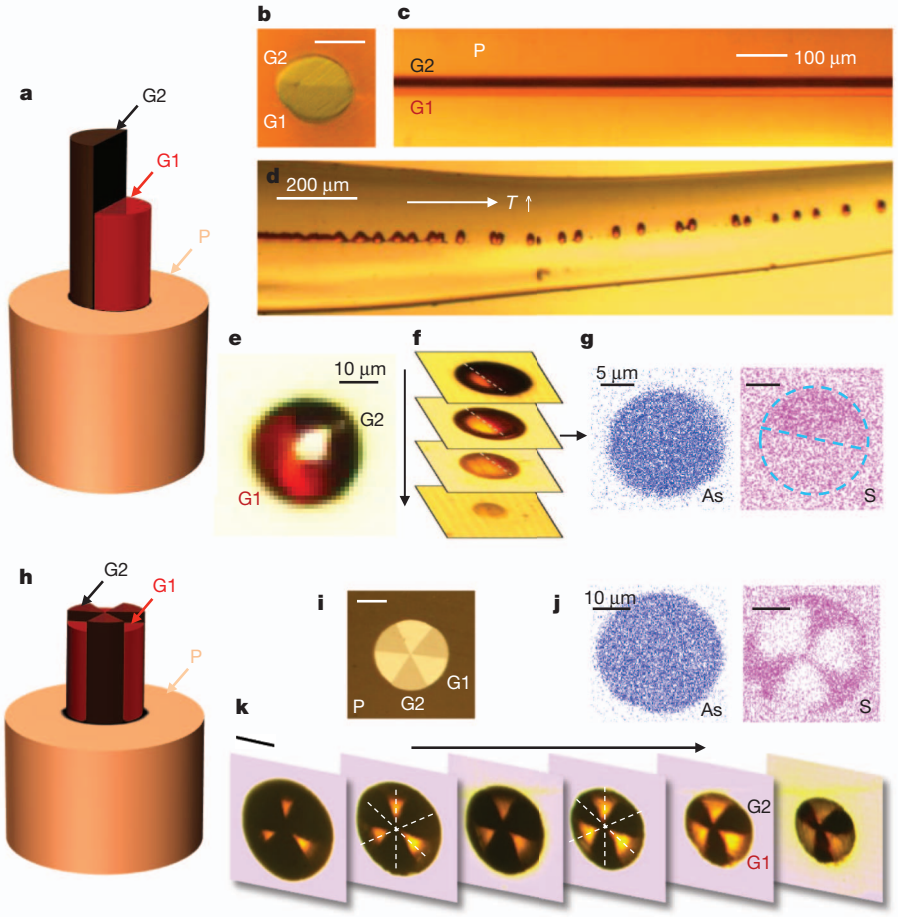

Figure 4 | Broken-symmetry Janus particle and 'beach ball' particle fabrication. **a**, Schematic of the Janus preform. G1, As_2S_3; G2, $(As_2Se_3)_{99}Ge_1$; P, PES. **b**, Reflection optical micrograph of a Janus fibre cross-section; scale bar 20 μm. **c**, Transmission optical micrograph of the fibre side view. **d**, Transmission optical micrograph showing PRI growth, leading to breakup of the Janus particles. **e**, Reflection optical micrograph of an individual Janus particle after removal from the fibre. **f**, Optical micrographs of multiple sections at different depths within a single Janus particle embedded in the fibre, exposed sequentially by polishing. The particle symmetry plane is tilted with respect to the direction of polishing, and the tilt is similar to that in the particle shown in **e**. **g**, EDX spectral images (for arsenic, As, and sulphur, S) of an exposed Janus particle cross-section, corresponding to a section from **f**. The dashed blue circle and line are visual aids. See Supplementary Fig. 8 for full EDX spectrum, Supplementary Fig. 9a–c for another example of EDX spectral imaging, and Supplementary Fig. 9d–f for a demonstration of Janus particle size-control. **h**, Schematic of the preform to produce 'beach ball' particles; G1, G2 and P as above. **i**, Reflection optical micrograph of a 'beach ball' fibre cross-section; scale bar, 20 μm. **j**, EDX spectral images (as in **g**) of an exposed 'beach ball' particle cross-section. **k**, Transmission optical micrographs of the cross-sections of a 40-μm-diameter particle immobilized in the polymer matrix in the fibre; scale bar 20 μm.

10^{14} 100-nm-diameter particles, well ordered in three dimensions. Particles are produced at the same volume rate regardless of the particle size, as it is inherently a three-dimensional process that relies only on the fibre fill factor.

Further control over the preform construction will result in particles with even more complex structures. This scalable process, in which we assemble disparate components that 'fit' together in size and shape macroscopically for the scalable production of size-tunable structured particles, enables a large range of applications. The well ordered, oriented and immobilized three-dimensional particle distribution in a scaffold (Supplementary Fig. 6) could potentially be used as three-dimensional optical and acoustic meta-materials; the surface-tension-driven smooth spherical surface morphology of the particles enables optical-resonance-based sensitive detection of chemical species and pathogens; and three-dimensional structural control over particles impregnated with drugs could help realize sophisticated controlled-release drug delivery systems.

Received 20 December 2011; accepted 2 May 2012.
Published online 18 July 2012.

1. Timko, B. P. *et al.* Advances in drug delivery. *Annu. Rev. Mater. Res.* **41,** 1–20 (2011).
2. Wang, J., Byrne, J. D., Napier, M. E. & DeSimone, J. M. More effective nanomedicines through particle design. *Small* **7,** 1919–1931 (2011).
3. Bell, A. T. The impact of nanoscience on heterogeneous catalysis. *Science* **299,** 1688–1691 (2003).
4. Souto, E. B. & Müller, R. H. Cosmetic features and applications of lipid nanoparticles. *Int. J. Cosmet. Sci.* **30,** 157–165 (2008).
5. Rotello, V. *Nanoparticles: Building Blocks for Nanotechnology* (Springer, 2003).
6. Li, T. (ed.) *Optical Fiber Communications* Vol. 1, *Fiber Fabrication* (Academic, 1985).
7. Eggers, J. & Villermaux, E. Physics of liquid jets. *Rep. Prog. Phys.* **71,** 036601 (2008).
8. Abouraddy, A. F. *et al.* Towards multimaterial multifunctional fibres that see, hear, sense and communicate. *Nature Mater.* **6,** 336–347 (2007).
9. Shabahang, S., Kaufman, J. J., Deng, D. S. & Abouraddy, A. F. Observation of the Plateau-Rayleigh capillary instability in multi-material optical fibers. *Appl. Phys. Lett.* **99,** 161909 (2011).
10. Sjöblom, J. *Encyclopedic Handbook of Emulsion Technology* (Marcel Dekker, 2001).
11. Walther, A. & Müller, A. H. E. Janus particles. *Soft Matter* **4,** 663–668 (2008).
12. Cao, G. *Nanostructures and Nanomaterials: Synthesis, Properties and Applications* (Imperial College Press, 2004).
13. Vollath, D. *Nanomaterials: An Introduction to Synthesis, Properties and Application* (Wiley-VCH, 2008).
14. Merkel, T. J. *et al.* Scalable shape-specific, top-down fabrication methods for the synthesis of engineered colloidal microparticles. *Langmuir* **26,** 13086–13096 (2010).
15. Utada, A. S. *et al.* Monodisperse double emulsions generated from a microcapillary device. *Science* **308,** 537–541 (2005).
16. Dendukuri, D. & Doyle, P. S. The synthesis and assembly of polymeric microparticles using microfluidics. *Adv. Mater.* **21,** 4071–4086 (2009).

17. Dendukuri, D., Pregibon, D. C., Collins, J., Hatton, T. A. & Doyle, P. S. Continuous-flow lithography for high-throughput microparticle synthesis. *Nature Mater.* **5,** 365–369 (2006).
18. Hernandez, C. J. & Mason, T. G. Colloidal alphabet soup: Monodisperse dispersions of shape-designed LithoParticles. *J. Phys. Chem. C* **111,** 4477–4480 (2007).
19. Rolland, J. P. *et al.* Direct fabrication and harvesting of monodisperse, shape specific nano-biomaterials. *J. Am. Chem. Soc.* **127,** 10096–10100 (2005).
20. Kaufman, J. J. *et al.* Thermal drawing of high-density macroscopic arrays of well-ordered sub-5-nm-diameter nanowires. *Nano Lett.* **11,** 4768–4773 (2011).
21. Nie, Z. H. *et al.* Emulsification in a microfluidic flow-focusing device: Effect of the viscosities of the liquids. *Microfluidics and Nanofluidics* **5,** 585–594 (2008).
22. Tomotika, S. On the instability of a cylindrical thread of a viscous liquid surrounded by another viscous fluid. *Proc. R. Soc. Lond. A* **150,** 322–337 (1935).
23. Deng, D. S. *et al.* In-fiber nanoscale semiconductor filament arrays. *Nano Lett.* **8,** 4265–4269 (2008).
24. Nisisako, T. & Torii, T. Microfluidic large-scale integration on a chip for mass production of monodisperse droplets and particles. *Lab Chip* **8,** 287–293 (2008).
25. Liang, X., Deng, D. S., Nave, J.-C. & Johnson, S. G. Linear stability analysis of capillary instabilities for concentric cylindrical shells. *J. Fluid Mech.* **683,** 235–262 (2011).
26. Deng, D. S., Nave, J.-C., Liang, X., Johnson, S. G. & Fink, Y. Exploration of in-fiber nanostructures from capillary instability. *Opt. Express* **19,** 16273–16290 (2011).
27. Smith, K. A., Solis, F. J. & Chopp, D. L. A projection method for motion of triple junctions by levels sets. *Interfaces Free Bound.* **4,** 263–276 (2002).
28. Dussan, V. E. B. On the spreading of liquids on solid surfaces: static and dynamic contact lines. *Annu. Rev. Fluid Mech.* **11,** 371–400 (1979).
29. de Gennes, P. G. Wetting: statics and dynamics. *Rev. Mod. Phys.* **57,** 827–863 (1985).
30. Israelachvili, J. N. *Intermolecular and Surface Forces* (Academic, 1992).
31. Ballato, J. *et al.* Advancements in semiconductor core optical fiber. *Opt. Fiber Technol.* **16,** 399–408 (2010).
32. Orf, N. D. *et al.* Fiber draw synthesis. *Proc. Natl Acad. Sci. USA* **108,** 4743–4747 (2011).

Supplementary Information is linked to the online version of the paper at www.nature.com/nature.

Acknowledgements Work at UCF was supported by the US National Science Foundation (award number ECCS-1002295), a Ralph E. Powe Junior Faculty Enhancement Award from the Oak Ridge Associated Universities (ORAU), in part by the US Air Force Office of Scientific Research (AFOSR) under contract FA-9550-12-1-0148, and by CREOL, The College of Optics & Photonics. Work at MIT was supported in part by the Materials Research Science and Engineering Program of the US NSF under award number DMR-0819762, and also in part by the US Army Research Office through the Institute for Soldier Nanotechnologies under contract number W911NF-07-D-0004. We thank Sasha Stolyarov, J. Manuel Perez, Sudipta Seal and Kirk Scammon for assistance. We especially thank M. J. Soileau, B. E. A. Saleh, D. N. Christodoulides and M. Z. Bazant for encouragement and support.

Author Contributions J.J.K., Y.F. and A.F.A. developed and directed the project. S.S. first observed the PRI phenomenon, developed the fibre tapering process and the particle extraction approach, and demonstrated the scale invariance of the PRI and particle extraction strategies. G.T. prepared and characterized all the glasses, carried out the preform extrusions, and produced the 'beach ball' fibre. J.J.K. produced the other preforms and fibres, performed PRI breakup and particle extraction experiments, and carried out the SEM, EDX, FIB and optical imaging and characterization. E.-H.B. aided in choice and characterization of materials and in preparation of the polymers. D.S.D., X.L. and S.G.J. carried out the theoretical calculations and performed the simulations. J.J.K., D.S.D., Y.F. and A.F.A. wrote the paper. All authors contributed to the interpretation of the results.

Author Information Reprints and permissions information is available at www.nature.com/reprints. The authors declare no competing financial interests. Readers are welcome to comment on the online version of this article at www.nature.com/nature. Correspondence and requests for materials should be addressed to A.F.A. (raddy@creol.ucf.edu).

CORRECTIONS & AMENDMENTS

ERRATUM
doi:10.1038/nature11454

Erratum: Structured spheres generated by an in-fibre fluid instability

Joshua J. Kaufman, Guangming Tao, Soroush Shabahang, Esmaeil-Hooman Banaei, Daosheng S. Deng, Xiangdong Liang, Steven G. Johnson, Yoel Fink & Ayman F. Abouraddy

Nature **487,** 463–467 (2012); doi:10.1038/nature11215

In this Letter, the received date was incorrectly listed as 20 December 2012 instead of 20 December 2011; this has been corrected in the HTML and PDF versions of the manuscript.